

Non-Orthogonal Multiple Access (NOMA) with Multiple Intelligent Reflecting Surfaces

Yanyu Cheng, *Student Member, IEEE*, Kwok Hung Li, *Senior Member, IEEE*,
Yuanwei Liu, *Senior Member, IEEE*, Kah Chan Teh, *Senior Member, IEEE*, and
George K. Karagiannidis, *Fellow, IEEE*

Abstract

In this paper, non-orthogonal multiple access (NOMA) networks assisted by multiple intelligent reflecting surfaces (IRSs) with discrete phase shifts are investigated, in which each user device (UD) is served by an IRS to improve the quality of the received signal. Two scenarios are considered based on whether there is a direct link or not between the base station (BS) and each UD, and the outage performance is analyzed for each of them. Specifically, the outage probability is approximated in the high signal-to-noise ratio (SNR) regime, and the diversity order is obtained. Orthogonal multiple access (OMA) can be regarded as a special case of NOMA, and the outage performance of the multi-IRS assisted OMA system is also characterized. It is demonstrated that NOMA outperforms OMA in multi-IRS assisted networks. Furthermore, it is shown that the use of discrete phase shifts does not degrade the diversity order. More importantly, simulation results further reveal that a 3-bit resolution for discrete phase shifts is sufficient to achieve near-optimal outage performance.

Index Terms

Discrete phase shift, intelligent reflecting surface (IRS), non-orthogonal multiple access (NOMA).

Y. Cheng, K. H. Li, and K. C. Teh are with the School of Electrical and Electronic Engineering, Nanyang Technological University, Singapore 639798 (e-mail: ycheng022@e.ntu.edu.sg; ekhli@ntu.edu.sg; ekcteh@ntu.edu.sg).

Y. Liu is with the School of Electronic Engineering and Computer Science, Queen Mary University of London, London E1 4NS, UK (e-mail: yuanwei.liu@qmul.ac.uk).

G. K. Karagiannidis is with the Department of Electrical and Computer Engineering, Aristotle University of Thessaloniki, Thessaloniki 54636, Greece (e-mail: geokarag@auth.gr).

I. INTRODUCTION

Non-orthogonal multiple access (NOMA) has been proposed as a candidate technique for future wireless communication networks [1]. The key idea of NOMA is to allocate multiple users to an orthogonal resource block, e.g., a time slot, a frequency band, a spreading code, but with different power levels [2], [3]. It has been demonstrated that NOMA outperforms the conventional orthogonal multiple access (OMA) from the aspects of spectral efficiency, connection density, and user fairness [4].

On the other hand, intelligent reflecting surfaces (IRSs) are envisioned to provide reconfigurable wireless environments for future communication networks, which are also named reconfigurable intelligent surfaces (RISs) and large intelligent surfaces (LISs) [5]. Specifically, an IRS consists of a large number of reconfigurable passive elements, and each element can induce a change of amplitude and phase for the incident signal [6], [7]. By appropriately adjusting amplitude-reflection coefficients and phase-shift variables, it can improve the link quality and enhance the coverage significantly [8]–[10]. Compared with the conventional communication assisting techniques such as relays, the IRS consumes less energy due to passive reflection and is able to operate in full-duplex (FD) mode without self-interference [11]. Therefore, IRSs have been proposed as a cost-effective solution to enhance the spectral and energy efficiency of future wireless communication networks [12], [13]. Also, IRSs have been introduced to NOMA networks for performance enhancement.

A. Related Work

NOMA: The performance of NOMA was first explored by simulations with different power allocation schemes, i.e., proportional fairness scheduler [14], tree-search based transmission power allocation [15], and fractional transmission power allocation [16], which demonstrated that NOMA outperforms the conventional OMA. In [17], Ding *et al.* evaluated the performance of a downlink NOMA system with randomly roaming users and showed that NOMA has better performance than OMA on the ergodic sum rate. Following that, Ding *et al.* studied the impact of user pairing on the sum rate of fixed-power-allocation NOMA and cognitive-radio-inspired NOMA systems [18]. In [19], Oviedo *et al.* demonstrated that NOMA using a fair power allocation approach can always outperform OMA in terms of the capacity for each user, regardless of channel conditions. In [20], Xu *et al.* proposed a new evaluation criterion to analyze the performance gain of NOMA over OMA. In [21], Liu *et al.* applied the simultaneous

wireless information and power transfer (SWIPT) to NOMA networks and proved that the use of SWIPT does not degrade the diversity order as compared to the conventional NOMA.

IRSs with continuous phase shifts: IRSs have attracted intensive research interest from both academia and industry [22], [23]. In [24], the superiority of an IRS was indicated as compared with a half-duplex (HD) decode-and-forward (DF) relay. In [25], the performance of a system aided by multiple IRSs was evaluated, and it was revealed that the IRS-aided system outperforms the FD DF relay (FDR)-aided system when the number of IRSs exceeds a certain value. Besides wireless communication systems, IRSs can also be applied to optical communication systems. In [26], it was revealed that the outage probability for an optical communication system can be reduced by introducing an IRS. Passive-beamforming design for IRSs is critical to system performance. In [27], multiple IRSs were deployed in a single-input single-output (SISO) system, and the phase shifts of IRSs were optimized by minimizing the outage probability. Active and passive beamforming were jointly optimized for IRS-aided multiple-input single-output (MISO) systems in [28], [29] with different objectives. For physical layer security, IRSs can also enhance system performance by blocking the signals of eavesdroppers [30], [31].

IRSs with discrete phase shifts: The aforementioned works assume that IRSs have continuous phase shifts. However, in practice, it is difficult to realize continuous phase shifts due to hardware limitations. Moreover, the complexity and cost will be extremely high especially when there are a large number of reflecting elements. Thus, it is more practical to consider discrete phase shifts for each reflecting element. In [32], the performance of an IRS-aided SISO system was evaluated from the data rate perspective. In [33], a MISO IRS-aided system with discrete phase shifts was considered, and the active beamforming at the BS and the passive beamforming at the IRS were jointly optimized to maximize the weighted sum rate. In [34], the uplink transmission for an IRS-aided system was studied. Specifically, the problems of the channel estimation and passive beamforming for the IRS with discrete phase shifts were investigated. In [35], the relation between the reflection amplitude and the phase shift was characterized, and the transmit power was minimized by designing active and passive beamforming. In [36] and [37], the transmit power was minimized by designing the continuous transmit beamforming at the BS and the discrete passive beamforming at the IRS. In [38], the symbol error rate was minimized by optimizing the precoding at the BS and the phase shifts at the IRS.

IRS-assisted NOMA: The combination of these two critical techniques, i.e., IRS and NOMA, has also been widely investigated. In [39], an IRS was deployed to improve the coverage by

assisting a cell-edge UD in data transmission, where this cell-edge user device (UD) is paired with a cell-center UD under the NOMA scheme. In [40], the impact of random phase shifting and coherent phase shifting for an IRS-aided NOMA system was further investigated. In [41] and [42], beamforming vectors of the base station (BS) and the IRS were optimized for an IRS-assisted NOMA system. The aforementioned works assumed that the BS-IRS-UD channel is non-line-of-sight (NLoS). Since the IRS can be pre-deployed, the path between the BS and the IRS may have line-of-sight (LoS) [43]–[45]. In [43], Yang *et al.* assumed the BS-IRS-UD link to be LoS and optimized the active and passive beamforming vectors for a NOMA system aided by an IRS. In [44], Liu *et al.* adopted machine learning approaches to jointly designing power allocation, passive beamforming, and the position of IRS for IRS-assisted NOMA systems. In [45], the IRS's parameters were designed for a prioritized UD in an IRS-assisted NOMA network.

B. Motivation and Contributions

The current works related to IRSs with discrete phase shifts mainly focus on optimizing beamforming vectors for IRS-assisted OMA systems [32]–[38]. Due to the consideration of IRSs with discrete phase shifts, it is a challenging task to evaluate system performance. This motivates us to characterize the performance of IRS-assisted NOMA and OMA systems with discrete phase shifts. On the other hand, a system assisted by multiple IRSs is also practical, and therefore, multiple IRSs are considered in this paper. The contributions are summarized as follows:

- We characterize the performance of multi-IRS aided NOMA networks with discrete phase shifts. More specifically, we consider two scenarios based on whether there are direct links between the BS and UDs or not.
- To be practical, we adopt the Nakagami- m fading model for the BS-UD, BS-IRS, and IRS-UD links so that these links can be either LoS or NLoS. Correspondingly, for each scenario, we derive the probability density function (PDF) and the cumulative distribution function (CDF) of the ordered channel gain by utilizing the Laplace transform.
- We approximate the outage probabilities in the high signal-to-noise ratio (SNR) regime for both scenarios. In addition, the outage probability of continuous phase shifts is also approximated for comparisons.
- To gain further insight, we obtain the diversity order for each scenario. We demonstrate that discrete phase shifts do not jeopardize the performance in terms of diversity order

as compared with continuous phase shifts. Simulation results further reveal that a 3-bit resolution for phase shifts is sufficient to achieve the near-optimal outage performance.

C. Outline and Notation

The remainder of this paper is organized as follows. In Section II, the system model of multi-IRS assisted NOMA with discrete phase shifts is described. The performance analysis of scenario I is conducted in Section III, followed by the analysis of scenario II in Section IV. Furthermore, numerical and simulation results are presented in Section V. Finally, our conclusion is drawn in Section VI.

In this paper, scalars are denoted by italic letters. Vectors and matrices are denoted by bold-face letters. For a vector \mathbf{v} , \mathbf{v}^T denotes the transpose of \mathbf{v} . $\text{diag}(\mathbf{v})$ denotes a diagonal matrix in which each diagonal element is the corresponding element in \mathbf{v} , respectively. $\arg(\cdot)$ denotes the argument of a complex number. $\mathbb{C}^{x \times y}$ denotes the space of $x \times y$ complex-valued matrices. $P_r(\cdot)$ denotes the probability.

II. SYSTEM MODEL

We consider a NOMA network assisted by multiple IRSs with discrete phase shifts. Specifically, there is a single-antenna BS and N IRSs, denoted by $\mathbf{R}_1, \mathbf{R}_2, \dots, \mathbf{R}_N$. All IRSs can be pre-deployed and have a sufficient distance from each other. Therefore, each IRS has a service coverage without overlapping with other IRSs' service areas, and the interference signals reflected from neighboring IRSs can be neglected due to the severe path loss [39]. Within the service area of each IRS, we select a single-antenna UD for this IRS. All N selected UDs, denoted by $\mathbf{U}_1, \mathbf{U}_2, \dots, \mathbf{U}_N$, form a NOMA group, and each UD is assisted by the corresponding IRS to communicate with the BS. Based on distances between the BS and all UDs, we consider two scenarios, scenario I and scenario II. More specifically, in scenario I, all UDs are far away from the BS, and there is no direct link between the BS and each UD as shown in Fig. 1(a), while in scenario II, all UDs can communicate with the BS directly as shown in Fig. 1(b). Each IRS has K discrete elements. The reflection-coefficient matrix of \mathbf{R}_n , denoted by $\Theta_n = \text{diag}(\beta_1^n e^{j\theta_1^n}, \beta_2^n e^{j\theta_2^n}, \dots, \beta_K^n e^{j\theta_K^n})$, can be intelligently adjusted by the IRS based on channel conditions, where $\beta_k^n \in (0, 1]$ and θ_k^n are the fixed amplitude reflection coefficient and the phase-shift variable of the k th element, respectively. To be practical, we consider discrete phase shifts which have b -bit resolution with

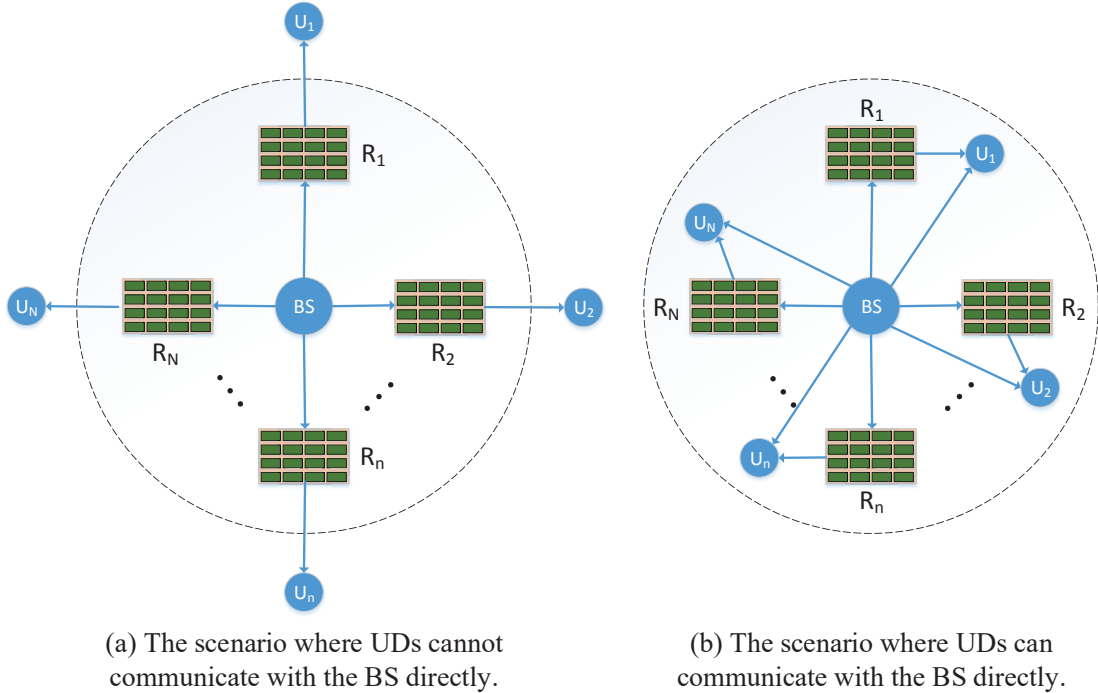


Fig. 1: The system models of multi-IRS assisted NOMA with discrete phase shifts for two scenarios.

$L = 2^b$ levels. By uniformly quantizing the interval $[0, 2\pi)$, we have the set of discrete phase-shift variables, $\mathcal{D} = \left\{ \frac{\Delta}{2}, \frac{3\Delta}{2}, \dots, \frac{(2L-1)\Delta}{2} \right\}$, where $\Delta = 2\pi/L$.

A. Channel Model

For both scenarios, all channels experience quasi-static flat fading, and the channel state information (CSI) of all channels is assumed to be perfectly known at the BS. The channel between the BS and R_n is denoted by $\mathbf{G}_n \in \mathbb{C}^{1 \times K}$. The channel between R_n and U_n is denoted by $\mathbf{g}_n \in \mathbb{C}^{K \times 1}$. Particularly, they are $\mathbf{G}_n = [G_1^n, G_2^n, \dots, G_K^n]$ and $\mathbf{g}_n = [g_1^n, g_2^n, \dots, g_K^n]^T$, respectively. All elements in \mathbf{G} and \mathbf{g} follow the Nakagami- m fading model with fading parameters m_G and m_g , respectively. For scenario II, besides BS-IRS-UD links, there are direct links between the BS and UDs. The channel between the BS and U_n is denoted by h_n , which follows the Nakagami- m fading model with the fading parameter m_h .

All links can be either LoS or NLoS for different scenarios. In particular, it is NLoS for $m_G = 1$ and it is LoS for $m_G > 1$ ($\mathcal{G} \in \{G, g, h\}$).

B. Signal Model

1) *Scenario I*: In scenario I, there is no direct link between the BS and each UD. Without loss of generality, assume that $|\mathbf{G}_1\Theta_1\mathbf{g}_1| \leq |\mathbf{G}_2\Theta_2\mathbf{g}_2| \leq \dots \leq |\mathbf{G}_N\Theta_N\mathbf{g}_N|$. The BS broadcasts the signal x which is given by

$$x = \sum_{n=1}^N \sqrt{\alpha_n P} s_n, \quad (1)$$

where P denotes the transmit power, s_n is the transmitted signal to U_n , α_n is the power allocation coefficients ($\alpha_1 > \alpha_2 > \dots > \alpha_N$, $\sum_{n=1}^N \alpha_n = 1$). The received signals at U_n is given by

$$y_n^1 = \mathbf{G}_n\Theta_n\mathbf{g}_n x + n_n, \quad (2)$$

where n_n is the additive white Gaussian noise (AWGN) at U_n . Based on the successive interference cancellation (SIC) principle, the signal-to-interference-plus-noise ratio (SINR) of detecting U_l 's signal at U_n ($l \leq n < N$ or $l < n = N$) is given by

$$\Psi_{n \leftarrow l}^1 = \frac{|\mathbf{G}_n\Theta_n\mathbf{g}_n|^2 \alpha_l}{|\mathbf{G}_n\Theta_n\mathbf{g}_n|^2 \sum_{i=l+1}^N \alpha_i + 1/\rho}, \quad (3)$$

where $\rho = P/\sigma_n^2$. As a special case, when $l = n = N$, the SNR of decoding U_N 's signal at U_N , is given by

$$\Psi_{N \leftarrow N}^1 = |\mathbf{G}_N\Theta_N\mathbf{g}_N|^2 \alpha_N \rho. \quad (4)$$

2) *Scenario II*: As compared with scenario I, the difference is that there are direct links between the BS and all UDs in scenario II. Without loss of generality, assume that $|h_1 + \mathbf{G}_1\Theta_1\mathbf{g}_1| \leq |h_2 + \mathbf{G}_2\Theta_2\mathbf{g}_2| \leq \dots \leq |h_N + \mathbf{G}_N\Theta_N\mathbf{g}_N|$. The received signal at U_n is given by

$$y_n^2 = (h_n + \mathbf{G}_n\Theta_n\mathbf{g}_n)x + n_n. \quad (5)$$

The SINR of detecting U_l 's signal at U_n ($l \leq n < N$ or $l < n = N$) is given by

$$\Psi_{n \leftarrow l}^2 = \frac{|h_n + \mathbf{G}_n\Theta_n\mathbf{g}_n|^2 \alpha_l}{|h_n + \mathbf{G}_n\Theta_n\mathbf{g}_n|^2 \sum_{i=l+1}^N \alpha_i + 1/\rho}. \quad (6)$$

For the special case of $l = n = N$, the SNR of decoding U_N 's signal at U_N , is given by

$$\Psi_{N \leftarrow N}^2 = |h_N + \mathbf{G}_N\Theta_N\mathbf{g}_N|^2 \alpha_N \rho. \quad (7)$$

III. THE SCENARIO WITHOUT DIRECT LINKS

In this section, we analyze the outage performance of scenario I. To derive the outage probability, the channel statistics are required.

A. IRS Parameters for Scenario I

When the direct link between the BS and each UD is not available, we aim to provide the best channel quality to each UD by adjusting the parameters of each IRS. For the BS-IRS- U_n link, it is to maximize $|\mathbf{G}_n \mathbf{\Theta}_n \mathbf{g}_n| = \left| \sum_{k=1}^K \beta_k^n G_k^n g_k^n e^{j\theta_k^n} \right|$ ($j = \sqrt{-1}$). This can be achieved by intelligently adjusting θ_k^n , the phase-shift variable of each element. By adjusting phase shifts of all $G_k^n g_k^n e^{j\theta_k^n}$ to be the same, we can obtain the optimal continuous phase-shift variables. There are more than one solution for $\{\theta_k^n\}$ ($k = 1, 2, \dots, K$), and the generalized solution is given by $\bar{\theta}_k^{1,n} = \tilde{\theta}_n - \arg(G_k^n g_k^n)$, where $\tilde{\theta}_n$ is an arbitrary constant ranging in $[0, 2\pi)$. After adopting optimal continuous phase shifts $\{\bar{\theta}_k^{1,n}\}$, we have

$$|\mathbf{G}_n \mathbf{\Theta}_n \mathbf{g}_n| = \beta \left| \sum_{k=1}^K G_k^n g_k^n e^{j\bar{\theta}_k^{1,n}} \right| = \beta \sum_{k=1}^K |G_k^n| |g_k^n|, \quad (8)$$

where we assume that $\beta_k^n = \beta$, $\forall n, k$, without loss of generality.

Since we consider discrete phase shifts, we can adjust the phase-shift variable of each element to be close to the optimal continuous phase-shift variable. Denote the optimal discrete phase-shift variable by $\hat{\theta}_k^{1,n}$. Then, we have

$$\hat{\theta}_k^{1,n} = \Delta \left(\left\lfloor \frac{\bar{\theta}_k^{1,n}}{\Delta} \right\rfloor + \frac{1}{2} \right), \quad (9)$$

where $\lfloor \cdot \rfloor$ is the floor function. The quantization error at the k th element is given by $\theta_k^{1,n,er} = \hat{\theta}_k^{1,n} - \bar{\theta}_k^{1,n}$, which is uniformly distributed in $[-\frac{\Delta}{2}, \frac{\Delta}{2})$. As such, after adopting the optimal discrete phase-shift variables $\{\hat{\theta}_k^{1,n}\}$, we can obtain the equivalent channel gain as

$$|\mathbf{G}_n \mathbf{\Theta}_n \mathbf{g}_n| = \beta \left| \sum_{k=1}^K G_k^n g_k^n e^{j\hat{\theta}_k^{1,n}} \right| = \beta \left| \sum_{k=1}^K G_k^n g_k^n e^{j\bar{\theta}_k^{1,n}} e^{j\theta_k^{1,n,er}} \right| = \beta \left| \sum_{k=1}^K |G_k^n| |g_k^n| e^{j\theta_k^{1,n,er}} \right|. \quad (10)$$

To verify our analysis of the optimal discrete phase shifts, we have conducted Monte Carlo simulations, and the results are shown in Fig. 2. It is observed that the ratio of the equivalent channel gain with discrete phase shifts to that with continuous phase shifts increases with the value of b , and gradually approaches 1.

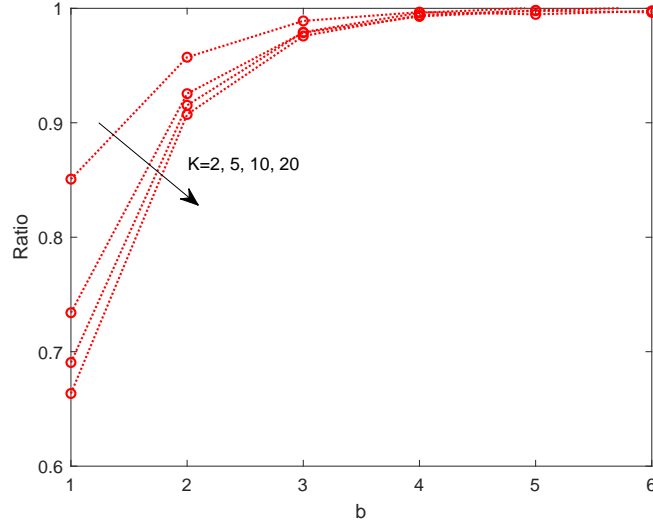


Fig. 2: The ratio of the average equivalent channel gain with discrete phase shifts to that with continuous phase shifts when $m_G = 2$, $m_g = 1$, and $\beta = 0.9$ in scenario I.

B. Channel Statistics without Direct Link

In [40] and [46], it is proved that the CLT-based channel statistics of the BS-IRS-UD link are inaccurate when the channel gain is near 0, and the Laplace transform is used to derive the accurate channel statistics for channel gain near 0. Therefore, we directly use the Laplace transform to derive new channel statistics before ordering, and then, we obtain the ordered channel statistics. For scenario I, the new channel statistics are shown in the following lemma.

Lemma 1. Denote that $Y_n = \beta \left| \sum_{k=1}^K |G_k^m| |g_k^n| e^{j\theta_k^{1,n,er}} \right|$ which is the n th channel gain in ascending order. Based on order statistics, when $m_G \neq m_g$ and $b \geq 2$, the CDF of Y_n for $y \rightarrow 0^+$ is approximated as

$$F_{Y_n}^{0^+}(y) \approx \frac{N!}{(N-n)!(n-1)!} \sum_{i=0}^{N-n} \binom{N-n}{i} \frac{(-1)^i}{n+i} \xi_1^{n+i} y^{2m_s K(n+i)}, \quad (11)$$

where $a = \beta \cos\left(\frac{\pi}{2b}\right)$, $m_s = \min\{m_G, m_g\}$, $m_l = \max\{m_G, m_g\}$, and

$$\xi_1 = \left(\frac{\sqrt{\pi} 4^{m_s - m_l + 1} (m_s m_l)^{m_s} \Gamma(2m_s) \Gamma(2m_l - 2m_s)}{\Gamma(m_s) \Gamma(m_l) \Gamma(m_l - m_s + \frac{1}{2})} \right)^K \frac{1}{2m_s K a^{2m_s K} \Gamma(2m_s K)}, \quad (12)$$

with $\Gamma(\cdot)$ denoting the gamma function. Note that equality holds when $b \rightarrow \infty$.

Proof. See Appendix A. ■

C. Performance Analysis of NOMA

The outage probability of U_n under the NOMA scheme is given by

$$\mathbb{P}_n^1 = 1 - \text{P}_r(\Psi_{n \leftarrow 1}^1 \geq \tilde{\gamma}_1, \Psi_{n \leftarrow 2}^1 \geq \tilde{\gamma}_2, \dots, \Psi_{n \leftarrow n}^1 \geq \tilde{\gamma}_n), \quad (13)$$

where $\tilde{\gamma}_i = 2^{\tilde{R}_i} - 1$ with \tilde{R}_i being the target rate of U_i . Furthermore, \mathbb{P}_n can be transformed into

$$\begin{aligned} \mathbb{P}_n^1 &= 1 - \text{P}_r(Y_n^2 \geq \tilde{\rho}_{n \leftarrow 1}, Y_n^2 \geq \tilde{\rho}_{n \leftarrow 2}, \dots, Y_n^2 \geq \tilde{\rho}_{n \leftarrow n}) \\ &= \text{P}_r(Y_n^2 < \tilde{\rho}_{n, \max}), \end{aligned} \quad (14)$$

where $\tilde{\rho}_{n, \max} = \max\{\tilde{\rho}_{n \leftarrow 1}, \tilde{\rho}_{n \leftarrow 2}, \dots, \tilde{\rho}_{n \leftarrow n}\}$ and

$$\tilde{\rho}_{n \leftarrow l} = \begin{cases} \frac{\tilde{\gamma}_l}{\rho \left(\alpha_l - \tilde{\gamma}_l \sum_{i=l+1}^N \alpha_i \right)}, & l \leq n < N \text{ or } l < n = N, \\ \frac{\tilde{\gamma}_N}{\rho \alpha_N}, & l = n = N. \end{cases} \quad (15)$$

Note that we need to ensure that $\alpha_l - \tilde{\gamma}_l \sum_{i=l+1}^N \alpha_i > 0$ for $1 \leq l \leq N - 1$.

Based on Lemma 1, we can derive the high-SNR approximation of the outage probability as shown in the following proposition.

Proposition 1. *Under the NOMA scheme in scenario I, the outage probability of U_n in the high-SNR regime when $b \geq 2$ is approximated as*

$$\mathbb{P}_n^{1, \infty} \approx \frac{N!}{(N-n)!n!} \xi_1^n \tilde{\rho}_{n, \max}^{nm_s K}. \quad (16)$$

Note that the approximation in the high-SNR regime is more accurate when b is larger.

Proof. First, we have

$$\mathbb{P}_n^{1, \infty} = F_{Y_n}^{0+} \left(\sqrt{\tilde{\rho}_{n, \max}} \right) \approx \frac{N!}{(N-n)!(n-1)!} \sum_{i=0}^{N-n} \binom{N-n}{i} \frac{(-1)^i}{n+i} \xi_1^{n+i} \tilde{\rho}_{n, \max}^{m_s K(n+i)}. \quad (17)$$

Then, after extracting the lowest-order term, we can obtain (16). This completes the proof. ■

Remark 1. Based on the proof of Lemma 1, the approximation error of (16) decreases as b increases.

Corollary 1. *In scenario I, when $b \geq 2$, the diversity order of the n th UD under the NOMA scheme is $nm_s K$.*

Proof. Since $\tilde{\rho}_{n, \max} \propto \rho^{-1}$, the diversity order can be determined as $nm_s K$ according to (16). This completes the proof. ■

Remark 2. In scenario I, the diversity order under the NOMA scheme is related to the number of IRS elements, Nakagami- m fading parameters of the BS-IRS-UD link, and the order of the channel gain.

The Special Case of $b \rightarrow \infty$: When $b \rightarrow \infty$, it is the special case of continuous phase shifts. In this case of scenario I, we can derive the high-SNR approximation of each UD's outage probability under the NOMA scheme for comparisons. The results are shown in the following proposition.

Proposition 2. *When the phase shifts are continuous, under the NOMA scheme in scenario I, the outage probability of U_n in the high-SNR regime is approximated as*

$$\mathbb{P}_n^{1,b \rightarrow \infty} = \frac{N!}{(N-n)!n!} \xi_2^n \tilde{\rho}_{n,max}^{nm_s K}, \quad (18)$$

where

$$\xi_2 = \left(\frac{\sqrt{\pi} 4^{m_s - m_l + 1} (m_s m_l)^{m_s} \Gamma(2m_s) \Gamma(2m_l - 2m_s)}{\Gamma(m_s) \Gamma(m_l) \Gamma(m_l - m_s + \frac{1}{2})} \right)^K \frac{1}{2m_s K \beta^{2m_s K} \Gamma(2m_s K)}. \quad (19)$$

Proof. When $b \rightarrow \infty$, we have $a \rightarrow \beta$. Then, we can obtain (18) after substituting $a \rightarrow \beta$ into (16). In addition, as mentioned in the proof of Lemma 1, the equality in (A.3) holds when $b \rightarrow \infty$. Hence, (18) is the asymptotic expression for U_n 's outage probability. This completes the proof. ■

Corollary 2. *In scenario I, for the special case of continuous phase shifts, the diversity order of the n th UD under the NOMA scheme is $nm_s K$.*

Remark 3. For scenario I, we observe that the multi-IRS assisted NOMA system with b -bit discrete phase shifts achieves the same diversity order as that with continuous phase shifts when $b \geq 2$, i.e., the application of discrete phase shifts does not jeopardize the diversity order.

D. Performance Analysis of OMA

We use Multi-IRS assisted OMA scheme as the benchmark for comparisons. Since there is no ordering for the channel gains in the OMA scheme, all UDs have the same outage probability. The outage probability of each UD is given by

$$\mathbb{P}_{OMA}^1 = \Pr(\Psi_{OMA}^1 < \tilde{\gamma}_{OMA}), \quad (20)$$

where $\Psi_{OMA}^1 = \rho |\mathbf{G}_n \Theta_n \mathbf{g}_n|^2$ and $\tilde{\gamma}_{OMA} = 2^{N\tilde{R}} - 1$. Furthermore, \mathbb{P}_{OMA}^1 can be transformed into

$$\mathbb{P}_{OMA}^1 = \Pr \left(Y^2 < \frac{\tilde{\gamma}_{OMA}}{\rho} \right), \quad (21)$$

where Y is the unordered equivalent channel gain.

Proposition 3. *Under the OMA scheme in scenario I, the outage probability of U_n in the high-SNR regime when $b \geq 2$ is approximated as*

$$\mathbb{P}_{OMA}^{1,\infty} \approx \xi_1 \tilde{\gamma}_{OMA}^{m_s K} \rho^{-m_s K}. \quad (22)$$

Note that the approximation in the high-SNR regime is more accurate when b is larger.

Proof. First, we have

$$\mathbb{P}_{OMA}^{1,\infty} = \Pr \left(Y < \sqrt{\frac{\tilde{\gamma}_{OMA}}{\rho}} \right) = F_Y^{0+} \left(\sqrt{\frac{\tilde{\gamma}_{OMA}}{\rho}} \right). \quad (23)$$

The PDF of Y has been derived in the proof of Lemma 1 as (A.12). Therefore, we can derive (22). This completes the proof. \blacksquare

Corollary 3. *In scenario I, when $b \geq 2$, the diversity order of each UD under the OMA scheme is $m_s K$.*

Remark 4. In scenario I, the diversity order under the OMA scheme is related to the number of IRS elements and Nakagami- m fading parameters of the BS-IRS-UD link.

The Special Case of $b \rightarrow \infty$: When $b \rightarrow \infty$, it is the special case of continuous phase shifts. In this case of scenario I, we can derive the high-SNR approximation of each UD's outage probability under the OMA scheme for comparisons, which is presented in the following proposition.

Proposition 4. *When the phase shifts are continuous, under the OMA scheme in scenario I, the outage probability of U_n in the high-SNR regime is approximated as*

$$\mathbb{P}_{OMA}^{1,b \rightarrow \infty} = \xi_2 \tilde{\gamma}_{OMA}^{m_s K} \rho^{-m_s K}. \quad (24)$$

Proof. It is similar to the proof of Proposition 2. \blacksquare

Corollary 4. *In scenario I, for the special case of continuous phase shifts, the diversity order of each UD under the OMA scheme is $m_s K$.*

Remark 5. For scenario I, we observe that the multi-IRS assisted OMA system with discrete phase shifts achieves the same diversity order as that with continuous phase shifts, i.e., the application of discrete phase shifts does not jeopardize the diversity order.

Remark 6. In scenario I, the lowest diversity order under the NOMA scheme is the same as the diversity order of each UD under the OMA scheme. Hence, in terms of the diversity order, the NOMA scheme outperforms the OMA scheme.

IV. THE SCENARIO WITH DIRECT LINKS

In this section, we analyze the outage performance of scenario II. To derive the outage probability, the channel statistics are required.

A. IRS Parameters for Scenario II

When there is a direct link between the BS and each UD, we need to maximize the equivalent channel gain between the BS and U_n , i.e., $|h_n + \mathbf{G}_n \Theta_n \mathbf{g}_n| = \left| h_n + \sum_{k=1}^K \beta_k^n G_k^n g_k^n e^{j\theta_k^n} \right|$. The optimal continuous phase shifts can be obtained by setting the phases of all $G_k^n g_k^n e^{j\theta_k^n}$ to be the same as h_n . For continuous phase shifts, there is only one solution that is given by $\bar{\theta}_k^{2,n} = \arg(h_n) - \arg(G_k^n g_k^n)$. After adopting the optimal continuous phase shifts $\{\bar{\theta}_k^{2,n}\}$, we have

$$|h_n + \mathbf{G}_n \Theta_n \mathbf{g}_n| = |h_n| + \beta \sum_{k=1}^K |G_k^n| |g_k^n|. \quad (25)$$

After considering discrete phase shifts, we can adjust the phase-shift variable of each element to be close to the optimal continuous phase-shift variable. Then, we have

$$\hat{\theta}_k^{2,n} = \Delta \left(\left\lfloor \frac{\bar{\theta}_k^{2,n}}{\Delta} \right\rfloor + \frac{1}{2} \right). \quad (26)$$

The quantization error is given by $\theta_k^{2,n,er} = \hat{\theta}_k^{2,n} - \bar{\theta}_k^{2,n}$, which is uniformly distributed in $[-\frac{\Delta}{2}, \frac{\Delta}{2})$. As such, after adopting the optimal discrete phase-shift variables $\{\hat{\theta}_k^{2,n}\}$, we can obtain the

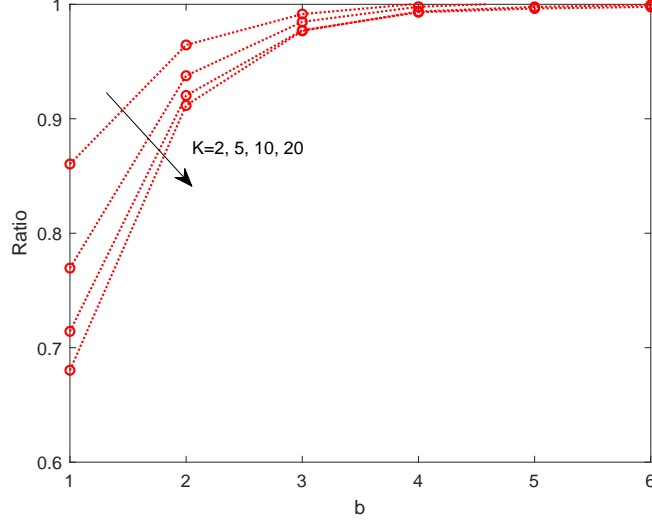


Fig. 3: The ratio of the average equivalent channel gain with discrete phase shifts to that with continuous phase shifts when $m_G = 2$, $m_g = 1$, $m_h = 1$, and $\beta = 0.9$ in scenario II.

channel gain as

$$\begin{aligned}
 |h_n + \mathbf{G}_n \Theta_n \mathbf{g}_n| &= \left| h_n + \beta \sum_{k=1}^K G_k^m g_k^n e^{j\hat{\theta}_k^{2,n}} \right| \\
 &= \left| |h_n| e^{j\arg(h_n)} + \beta \sum_{k=1}^K |G_k^m| |g_k^n| e^{j\arg(G_k^m g_k^n)} e^{j\bar{\theta}_k^{2,n}} e^{j\theta_k^{2,n,er}} \right| \\
 &= \left| |h_n| + \beta \sum_{k=1}^K |G_k^m| |g_k^n| e^{j\theta_k^{2,n,er}} \right|.
 \end{aligned} \tag{27}$$

To verify our analysis of the optimal discrete phase shifts, we have conducted Monte Carlo simulations, and the results are shown in Fig. 3. It is observed that the ratio of the equivalent channel gain with discrete phase shifts to that with continuous phase shifts increases with the value of b , and gradually approaches 1.

B. Channel Statistics with Direct Link

For scenario II, the new channel statistics for channel gain near 0 are shown in the following lemma.

Lemma 2. Denote that $Z_n = \left| |h_n| + \beta \sum_{k=1}^K |G_k^n| |g_k^n| e^{j\theta_k^{2,n,er}} \right|$ which is the n th channel gain in the ascending order. Based on order statistics, when $m_G \neq m_g$ and $b \geq 2$, the CDF of Z_n for $z \rightarrow 0^+$ is approximated as

$$F_{Z_n}^{0+}(z) \approx \frac{N!}{(N-n)!(n-1)!} \sum_{i=0}^{N-n} \binom{N-n}{i} \frac{(-1)^i}{n+i} \xi_3^{n+i} z^{(2m_h+2m_sK)(n+i)}, \quad (28)$$

where

$$\begin{aligned} \xi_3 = & \left(\frac{\sqrt{\pi} 4^{m_s-m_l+1} (m_s m_l)^{m_s} \Gamma(2m_s) \Gamma(2m_l - 2m_s)}{\Gamma(m_s) \Gamma(m_l) \Gamma(m_l - m_s + \frac{1}{2})} \right)^K \\ & \times \frac{\Gamma(2m_h) (2m_h)^{m_h}}{(2m_h + 2m_s K) a^{K-2m_s K} \Gamma(m_h) \Gamma(2m_h + 2m_s K)}. \end{aligned} \quad (29)$$

Note that equality holds when $b \rightarrow \infty$.

Proof. See Appendix B. ■

C. Performance Analysis of NOMA

In scenario II, the outage probability of U_n under the NOMA scheme is given by

$$\mathbb{P}_n^2 = 1 - \text{Pr}(\Psi_{n \leftarrow 1}^2 \geq \tilde{\gamma}_1, \Psi_{n \leftarrow 2}^2 \geq \tilde{\gamma}_2, \dots, \Psi_{n \leftarrow n}^2 \geq \tilde{\gamma}_n), \quad (30)$$

where $\tilde{\gamma}_i = 2^{\tilde{R}_i} - 1$ with \tilde{R}_i being the target rate of U_i . Furthermore, \mathbb{P}_n can be transformed into

$$\mathbb{P}_n^2 = 1 - \text{Pr}(Z_n^2 \geq \tilde{\rho}_{n \leftarrow 1}, Z_n^2 \geq \tilde{\rho}_{n \leftarrow 2}, \dots, Z_n^2 \geq \tilde{\rho}_{n \leftarrow n}) = \text{Pr}(Z_n^2 < \tilde{\rho}_{n,max}). \quad (31)$$

Based on Lemma 2, we can derive the high-SNR approximation of the outage probability as shown in the following proposition.

Proposition 5. Under the NOMA scheme in scenario II, the outage probability of U_n in the high-SNR regime when $b \geq 2$ is approximated as

$$\mathbb{P}_n^{2,\infty} \approx \frac{N!}{(N-n)!n!} \xi_3^n \tilde{\rho}_{n,max}^{n(m_h+m_sK)}. \quad (32)$$

Note that the approximation in the high-SNR regime is more accurate when b is larger.

Proof. First, we have

$$\mathbb{P}_n^{2,\infty} = F_{Z_n}^{0+}(\sqrt{\tilde{\rho}_{n,max}}) \approx \frac{N!}{(N-n)!(n-1)!} \sum_{i=0}^{N-n} \binom{N-n}{i} \frac{(-1)^i}{n+i} \xi_3^{n+i} \tilde{\rho}_{n,max}^{(m_h+m_sK)(n+i)}. \quad (33)$$

Then, after extracting the lowest-order term, we can derive (32). This completes the proof. ■

Remark 7. Based on the proof of Lemma 2, the approximation error of (32) decreases as b increases.

Corollary 5. *In scenario II, when $b \geq 2$, the diversity order of the n th UD under the NOMA scheme is $n(m_h + m_s K)$.*

Proof. Since $\tilde{\rho}_{n,max} \propto \rho^{-1}$, the diversity order can be determined as $n(m_h + m_s K)$ according to (32). This completes the proof. ■

Remark 8. In scenario II, the diversity order under the NOMA scheme is related to the number of IRS elements, the Nakagami- m fading parameter of the direct link, Nakagami- m fading parameters of the BS-IRS-UD link, and the order of the channel gain.

The Special Case of $b \rightarrow \infty$: When $b \rightarrow \infty$, it is the special case of continuous phase shifts. In this case of scenario II, we can derive the high-SNR approximation of each UD's outage probability under the NOMA scheme for comparisons. The results are shown in the following proposition.

Proposition 6. *When the phase shifts are continuous, under the NOMA scheme in scenario II, the outage probability of U_n in the high-SNR regime is approximated as*

$$\mathbb{P}_n^{b \rightarrow \infty} = \frac{N!}{(N-n)!n!} \xi_4^n \tilde{\rho}_{n,max}^{n(m_h + m_s K)}, \quad (34)$$

where

$$\xi_4 = \left(\frac{\sqrt{\pi} 4^{m_s - m_l + 1} (m_s m_l)^{m_s} \Gamma(2m_s) \Gamma(2m_l - 2m_s)}{\Gamma(m_s) \Gamma(m_l) \Gamma(m_l - m_s + \frac{1}{2})} \right)^K \times \frac{\Gamma(2m_h) (2m_h)^{m_h}}{(2m_h + 2m_s K) \beta^{K-2m_s K} \Gamma(m_h) \Gamma(2m_h + 2m_s K)}. \quad (35)$$

Proof. When $b \rightarrow \infty$, we have $a \rightarrow \beta$. Then, we can obtain (34) after substituting $a \rightarrow \beta$ into (32). In addition, as mentioned in the proof of Lemma 2, the equality in (B.1) holds when $b \rightarrow \infty$. Hence, (34) is the asymptotic expression for U_n 's outage probability. This completes the proof. ■

Corollary 6. *In scenario II, for the special case of continuous phase shifts, the diversity order the n th UD under the NOMA scheme is $n(m_h + m_s K)$.*

Remark 9. For scenario II, we observe that the multi-IRS assisted NOMA system with b -bit discrete phase shifts achieves the same diversity order as that with continuous phase shifts when $b \geq 2$, i.e., the application of discrete phase shifts does not jeopardize the diversity order.

D. Performance Analysis of OMA

Since there is no ordering for the channel gains in the OMA scheme, all UDs have the same outage probability. The outage probability of U_n is given by

$$\mathbb{P}_{OMA}^2 = \Pr(\Psi_{OMA}^2 < \tilde{\gamma}_{OMA}), \quad (36)$$

where $\Psi_{OMA}^2 = \rho|h_n + \mathbf{G}_n \Theta_n \mathbf{g}_n|^2$. Furthermore, \mathbb{P}_{OMA}^2 can be transformed into

$$\mathbb{P}_{OMA}^2 = \Pr\left(Z^2 < \frac{\tilde{\gamma}_{OMA}}{\rho}\right), \quad (37)$$

where Z is the unordered equivalent channel gain.

Proposition 7. *Under the OMA scheme in scenario II, the outage probability of U_n in the high-SNR regime when $b \geq 2$ is approximated as*

$$\mathbb{P}_{OMA}^{2,\infty} \approx \xi_3 \tilde{\rho}_{n \leftarrow n}^{m_h + m_s K}. \quad (38)$$

Note that the approximation in the high-SNR regime is more accurate when b is larger.

Proof. First, we have

$$\mathbb{P}_{OMA}^{2,\infty} = \Pr\left(Z < \sqrt{\frac{\tilde{\gamma}_{OMA}}{\rho}}\right) = F_Z^{0+}\left(\sqrt{\frac{\tilde{\gamma}_{OMA}}{\rho}}\right). \quad (39)$$

The PDF of Z has been derived in the proof of Lemma 2 as (B.11). Therefore, we can derive (38). This completes the proof. \blacksquare

Corollary 7. *In scenario II, when $b \geq 2$, the diversity order of each UD under the OMA scheme is $m_h + m_s K$.*

Remark 10. In scenario II, the diversity order under the OMA scheme is related to the number of IRS elements, the Nakagami- m fading parameter of the direct link, and Nakagami- m fading parameters of the BS-IRS-UD link.

The Special Case of $b \rightarrow \infty$: When $b \rightarrow \infty$, it is the special case of continuous phase shifts. In this case of scenario II, we can derive the high-SNR approximation of each UD's

outage probability under the OMA scheme for comparison, which is presented in the following proposition.

Proposition 8. *When the phase shifts are continuous, under the OMA scheme in scenario II, the outage probability of U_n in the high-SNR regime is approximated as*

$$\mathbb{P}_{OMA}^{2,b \rightarrow \infty} = \xi_4 \tilde{\rho}_{n \leftarrow n}^{m_h + m_s K}. \quad (40)$$

Proof. It is similar to the proof of Proposition 6. ■

Corollary 8. *In scenario II, for the special case of continuous phase shifts, the diversity order of each UD under the OMA scheme is $m_h + m_s K$.*

Remark 11. For scenario II, we observe that the multi-IRS assisted OMA system with discrete phase shifts achieves the same diversity order as that with continuous phase shifts, i.e., the application of discrete phase shifts does not jeopardize the diversity order.

Remark 12. In scenario II, the lowest diversity order under the NOMA scheme is the same as the diversity order of each UD under the OMA scheme. Hence, in terms of the diversity order, the NOMA scheme outperforms the OMA scheme.

E. Summary of Diversity Orders

After completing all analyses for both scenarios, all results are summarized in Table I for ease of reference.

TABLE I: Diversity order of U_n (the n th UD) for each scenario

Multiple access scheme	NOMA		OMA	
	Discrete	Continuous	Discrete	Continuous
Scenario I	$nm_s K$	$nm_s K$	$m_s K$	$m_s K$
Scenario II	$n(m_h + m_s K)$	$n(m_h + m_s K)$	$m_h + m_s K$	$m_h + m_s K$

We observe that the discrete phase shifts can achieve the same diversity order as the continuous phase shifts, but with lower hardware complexity and cost.

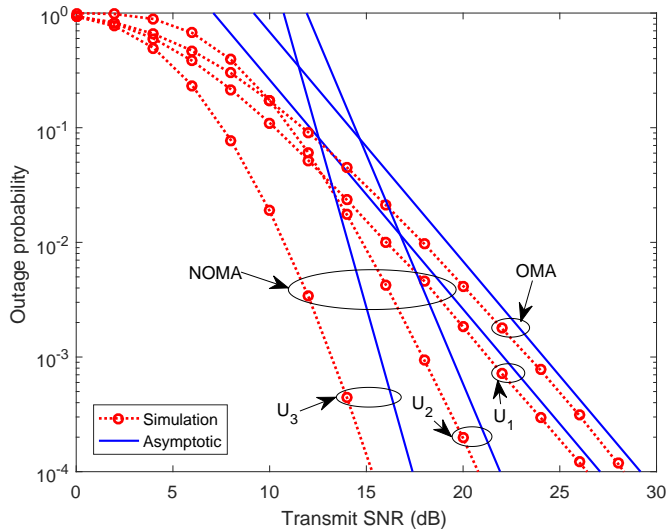


Fig. 4: Outage probability versus SNR in scenario I when $K = 2$ and $b = 3$.

V. NUMERICAL RESULTS

In this section, numerical results are presented for the performance evaluation of the considered network. Meanwhile, Monte Carlo simulations are conducted to verify the accuracy. The parameters are shown in Table II.

TABLE II: Parameters setting

Number of IRSs and UDs	$N = 3$
Amplitude-reflection coefficient of the IRS	$\beta = 0.9$
Nakagami- m fading parameters	$m_G = 2$, $m_g = 1$, and $m_h = 1$
Power-allocation coefficients for the downlink	$\alpha_1 = 0.7$, $\alpha_2 = 0.2$, and $\alpha_3 = 0.1$
Target data-rates for the fixed-rate transmission	$\tilde{R} = 1$ bps/Hz

A. Scenario I

In Fig. 4, outage probabilities versus the transmit SNR in scenario I when $K = 2$ and $b = 3$ are plotted. There are three UDs in a NOMA group. First, we observe that the outage probability of each UD for NOMA gradually approaches its high-SNR approximation curve that is derived from (16), which validates our analysis. Then, by observing the slopes, the diversity orders of

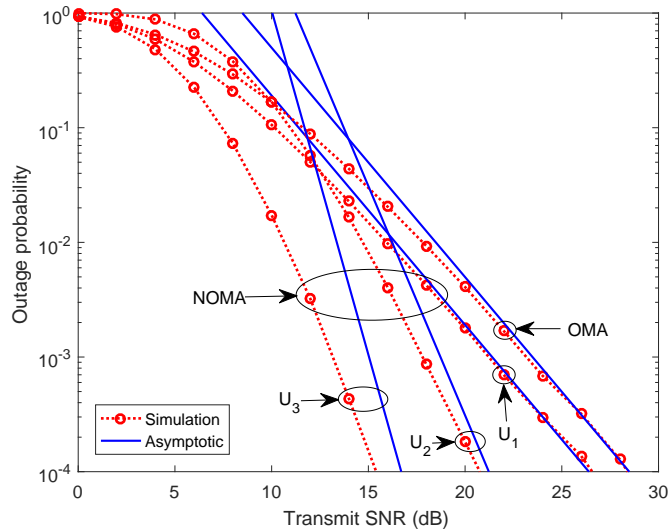


Fig. 5: Outage probability versus SNR in scenario I when $K = 2$ and $b \rightarrow \infty$ (continuous phase shifts).

U_1 , U_2 , and U_3 are 2, 4, and 6, respectively, which is consistent with Corollary 1. On the other hand, the outage probability for OMA is plotted with the high-SNR approximation curve that is derived from (22). There is only one curve for OMA, as these three UDs have the same outage probability statistically. It is observed that the diversity order for OMA is 2, which validates Corollary 3. This observation demonstrates the superiority of NOMA over OMA from the diversity order perspective.

Then, we increase b to approach ∞ , which is the special case of continuous phase shifts, and the outage probability versus the transmit SNR is plotted in Fig. 5. It is observed that all outage probability curves approach their respective asymptotic curves that are derived from (18) and (24). It is also observed that the diversity orders of U_1 , U_2 , and U_3 in the NOMA scheme are 2, 4, and 6, respectively, while the diversity order for OMA with continuous phase shifts is 2. This observation is consistent with Corollary 2 and 4. The diversity orders of UDs with continuous phase shifts are the same as those with discrete phase shifts. It is revealed that the discrete phase shifts do not degrade the diversity order as compared with the continuous phase shifts.

In Fig. 6, the outage probability of U_1 versus the number of IRS elements in scenario I is plotted. First, we observe that the outage probability decreases as K increases. Then, we observe that the outage probability for $\rho = 6$ dB is lower than that for $\rho = 3$ dB. Next, we observe that

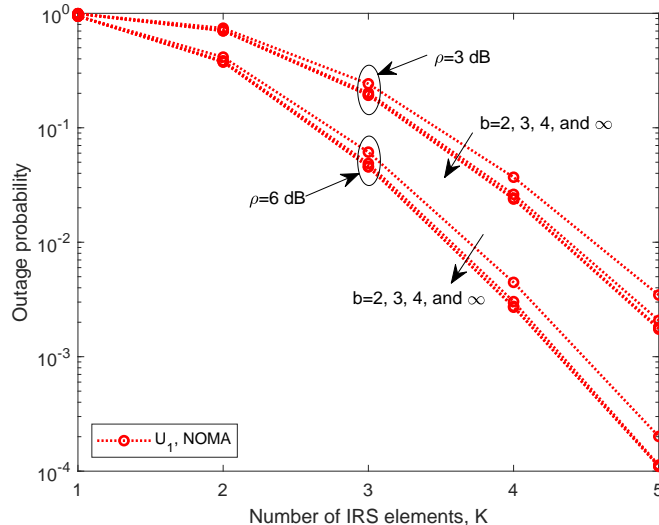


Fig. 6: Outage probability of U_1 versus K in scenario I when $\rho = 3$ dB and 6 dB.

for each specific transmit SNR, the outage probability increases with the increase of b . More importantly, when $b \geq 3$, the outage probability is close to the outage probability of continuous phase shifts. It reveals that 3-bit resolution for phase shifts is sufficient to achieve near-optimal performance.

B. Scenario II

The outage probabilities versus the transmit SNR in scenario II when $K = 2$ and $b = 3$ are plotted in Fig. 7. There are three UDs in a NOMA group. First, we observe that the outage probability of each UD for NOMA gradually approaches its high-SNR approximation curve that is derived from (32), which validates our analysis. Then, by observing the slopes, the diversity orders of U_1 , U_2 , and U_3 are 3, 6, and 9, respectively, which is consistent with Corollary 5. On the other hand, the outage probability for OMA is plotted with the high-SNR approximation curve that is derived from (38). There is only one curve for OMA, as these three UDs have the same outage probability statistically. It is observed that the diversity order for OMA is 3, which validates Corollary 7. This observation demonstrates that NOMA outperforms OMA from the diversity order perspective.

Then, we increase b to approach ∞ , which is the special case of continuous phase shifts, and the outage probability curve is plotted in Fig. 8. It is observed that all outage probability

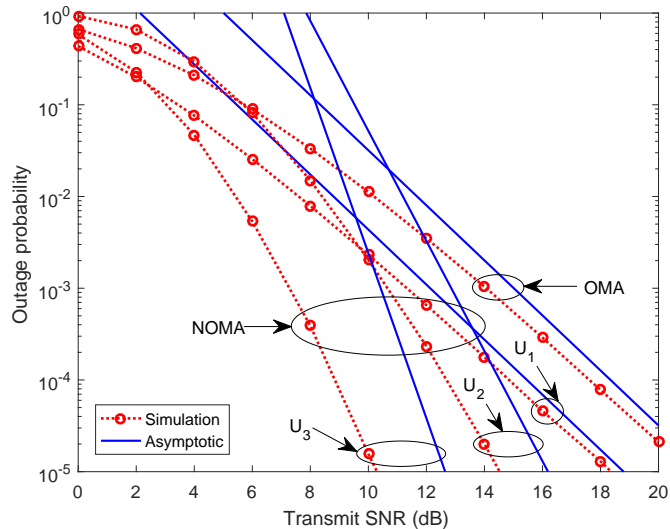


Fig. 7: Outage probability versus SNR in scenario II when $K = 2$ and $b = 3$.

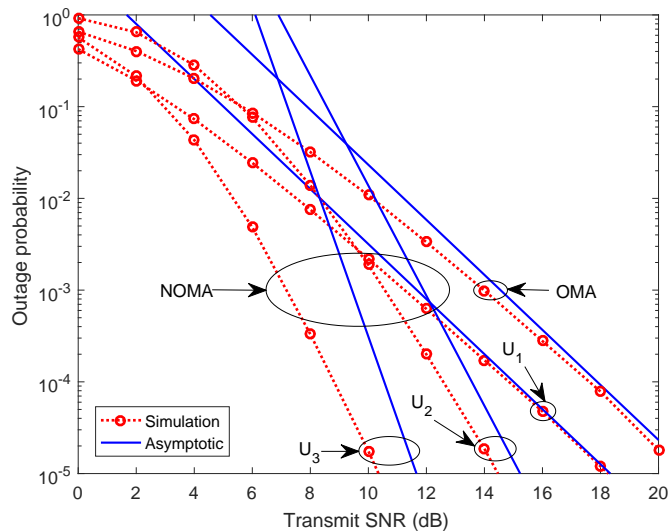


Fig. 8: Outage probability versus SNR in scenario II when $K = 2$ and $b \rightarrow \infty$ (continuous phase shifts).

curves approach their respective asymptotic curves, that are derived from (34) and (40). It is also observed that the diversity orders of U_1 , U_2 , and U_3 in the NOMA scheme are 3, 6, and 9, respectively, while the diversity order for OMA with continuous phase shifts is 3. This

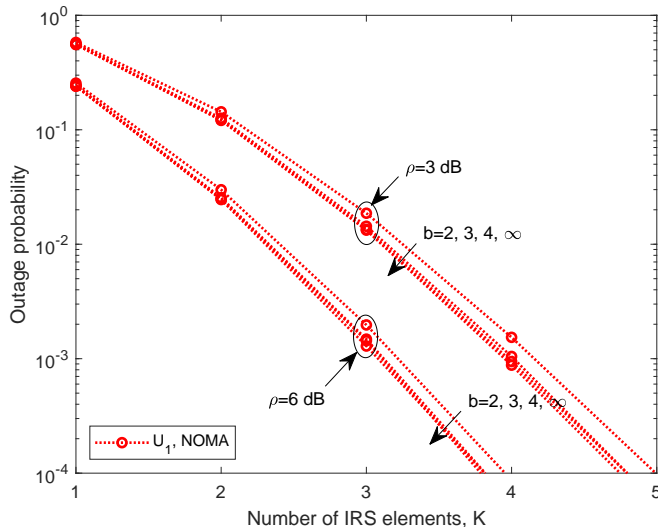


Fig. 9: Outage probability of U_1 versus K in scenario II when $\rho = 3$ dB and 6 dB.

observation is consistent with Corollary 6 and 8. The diversity orders of UDs with continuous phase shifts are the same as those with discrete phase shifts. It is revealed that when direct links are considered, the discrete phase shifts also do not degrade the diversity order as compared with the continuous phase shifts.

In Fig. 9, the outage probability of U_1 versus the number of IRS elements scenario II is plotted. First, we observe that the outage probability decreases as K increases. Then, we observe that the outage probability for $\rho = 6$ dB is lower than that for $\rho = 3$ dB. Next, we observe that for each specific transmit SNR, the outage probability increases with the increase of b . Importantly, when $b \geq 3$, the outage probability is close to the outage probability of continuous phase shifts. It is revealed that when direct links are considered, a 3-bit resolution is also sufficient for phase shifts to achieve near-optimal performance.

VI. CONCLUSIONS

In this paper, we have studied multi-IRS assisted NOMA systems with discrete phase shifts. For each scenario, new channel statistics have been derived. Following that, the high-SNR approximation of the outage probability has been derived. Furthermore, the diversity order for each scenario has been determined to provide insight into the performance. Most importantly, it has been demonstrated that the diversity order of discrete phase shifts is the same as that of

continuous phase shifts for each scenario. Furthermore, it has been shown that a 3-bit resolution is sufficient for discrete phase shifts to achieve the near-optimal performance for each scenario. Therefore, IRSs with discrete phase shifts can strike a balance between system performance and hardware cost. As the CSI is assumed to be perfectly known at the BS in this paper, IRS-assisted networks with imperfect CSI are worth investigating for future work.

APPENDIX A
PROOF OF LEMMA 1

Unordered channel gain: First, we need to derive the PDF of the unordered channel gain which is denoted by Y . Then, we have the channel gain after adopting the optimal discrete phase shifts $\{\hat{\theta}_k^n\}$ for any n as

$$Y = \beta \left| \sum_{k=1}^K |G_k^n| |g_k^n| e^{j\theta_k^{1,n,er}} \right| = \beta \left| \sum_{k=1}^K |G_k^n| |g_k^n| (\cos(\theta_k^{1,n,er}) + j \sin(\theta_k^{1,n,er})) \right|. \quad (\text{A.1})$$

Since $\theta_k^{1,n,er}$ is uniformly distributed in $[-\frac{\Delta}{2}, \frac{\Delta}{2})$, we have

$$Y \approx \beta \sum_{k=1}^K |G_k^n| |g_k^n| \cos(\theta_k^{1,n,er}), \quad (\text{A.2})$$

where the equality holds when $\Delta \rightarrow 0$. When b is relatively large, we can further approximate Y as

$$Y \approx a \sum_{k=1}^K |G_k^n| |g_k^n|, \quad (\text{A.3})$$

where the equality holds when $b \rightarrow \infty$. Next, we denote $Q = \sum_{k=1}^K Q_k$, where $Q_k = |G_k^n| |g_k^n|$. Since all Q_k ($k = 1, 2, \dots, K$) are i.i.d., according to [47], the PDF of single Q_k (the product of two Nakagami- m random variables) is given by

$$f_{Q_k}(q) = \frac{4(m_s m_l)^{\frac{m_s+m_l}{2}}}{\Gamma(m_s)\Gamma(m_l)} q^{m_s+m_l-1} K_{m_s-m_l}(2\sqrt{m_s m_l}q), \quad (\text{A.4})$$

for $q \geq 0$, where $K_v(\cdot)$ is the modified Bessel function of the second kind. The Laplace transform of $f_{Q_k}(q)$ is derived as

$$\mathcal{L}_{f_{Q_k}}(s) = \frac{4(m_s m_l)^{\frac{m_s+m_l}{2}}}{\Gamma(m_s)\Gamma(m_l)} \int_0^\infty q^{m_s+m_l-1} e^{-sq} K_{m_s-m_l}(2\sqrt{m_s m_l}q) dq. \quad (\text{A.5})$$

Furthermore, by referring to [48, eq. (6.621.3)], we have

$$\mathcal{L}_{f_{Q_k}}(s) = \phi_1(s + 2\sqrt{m_s m_l})^{-2m_s} F\left(2m_s, m_s - m_l + \frac{1}{2}; m_s + m_l + \frac{1}{2}; \frac{s - 2\sqrt{m_s m_l}}{s + 2\sqrt{m_s m_l}}\right), \quad (\text{A.6})$$

where $\phi_1 = \frac{\sqrt{\pi}4^{m_s-m_l+1}(m_s m_l)^{m_s}\Gamma(2m_s)\Gamma(2m_l)}{\Gamma(m_s)\Gamma(m_l)\Gamma(m_s+m_l+\frac{1}{2})}$ and $F(\cdot, \cdot; \cdot; \cdot)$ is the hypergeometric series. When $s \rightarrow \infty$, since $m_s < m_l$ satisfies the condition of [48, eq. (9.122.1)], we have

$$\mathcal{L}_{f_{Q_k}}^\infty(s) = \phi_2 s^{-2m_s}, \quad (\text{A.7})$$

where $\phi_2 = \frac{\sqrt{\pi}4^{m_s-m_l+1}(m_s m_l)^{m_s}\Gamma(2m_s)\Gamma(2m_l-2m_s)}{\Gamma(m_s)\Gamma(m_l)\Gamma(m_l-m_s+\frac{1}{2})}$. Since all Q_k are i.i.d., we have

$$\mathcal{L}_{f_Q}^\infty(s) = \prod_{k=1}^K \mathcal{L}_{f_{Q_k}}^\infty(s) = \phi_2^K s^{-2m_s K}. \quad (\text{A.8})$$

Thus, by performing the inverse Laplace transform for (A.8) and referring to [48, eq. (17.13.3)], the PDF of Q for $q \rightarrow 0^+$ can be derived as

$$f_Q^{0+}(q) = \frac{\phi_2^K}{\Gamma(2m_s K)} q^{2m_s K - 1}, \quad (\text{A.9})$$

for $q \geq 0$. Following that, according to [48, eq. (3.351.1)], the CDF of Q for $q \rightarrow 0^+$ can be derived as

$$F_Q^{0+}(q) = \frac{\phi_2^K}{\Gamma(2m_s K) 2m_s K} q^{2m_s K}, \quad (\text{A.10})$$

for $q \geq 0$. Finally, the PDF and the CDF of Y can be approximated as

$$f_Y^{0+}(y) \approx \frac{1}{a} f_Q^{0+}\left(\frac{y}{a}\right) = \phi_3 y^{2m_s K - 1}, \quad (\text{A.11})$$

and

$$F_Y^{0+}(y) \approx F_Q^{0+}\left(\frac{y}{a}\right) = \xi_1 y^{2m_s K}, \quad (\text{A.12})$$

respectively, for $y \geq 0$, where $\phi_3 = \frac{\phi_2^K}{\Gamma(2m_s K) a^{2m_s K}}$ and $\xi_1 = \frac{\phi_3}{2m_s K}$.

Ordered channel gain: Based on order statistics [49], the PDF of Y_n can be approximated as

$$F_{Y_n}^{0+}(y) \approx \frac{N!}{(N-n)!(n-1)!} \sum_{i=0}^{N-n} \binom{N-n}{i} \frac{(-1)^i}{n+i} \left(F_Y^{0+}(y)\right)^{n+i}. \quad (\text{A.13})$$

This completes the proof.

APPENDIX B
PROOF OF LEMMA 2

Unordered channel gain: First, we need to derive the PDF of the unordered channel gain which is denoted by Z . Then, similar to the proof of Lemma 1, when b is relatively large, we have

$$Z \approx |h_n| + \beta \sum_{k=1}^K |G_k^m| |g_k^n| \cos(\theta_k^{2,n,er}) \approx |h_n| + a \sum_{k=1}^K |G_k^n| |g_k^n|, \quad (\text{B.1})$$

where the equality holds when $b \rightarrow \infty$. Since h_n follows the Nakagami- m fading model, the PDF of the unordered $|h_n|$ is given by

$$f_{|h_n|}(x) = \frac{2m_h^{m_h}}{\Gamma(m_h)} x^{2m_h-1} e^{-m_h x^2}. \quad (\text{B.2})$$

The Laplace transform of $f_{|h_n|}(x)$ is given by

$$\mathcal{L}_{f_{|h_n|}}(s) = \frac{2m_h^{m_h}}{\Gamma(m_h)} \int_0^\infty x^{2m_h-1} e^{-m_h x^2} e^{-sx} dx. \quad (\text{B.3})$$

Then, by referring to [48, eq. (3.462.1)], we can derive that

$$\mathcal{L}_{f_{|h_n|}}(s) = \frac{\Gamma(2m_h)}{\Gamma(m_h)} e^{\frac{s^2}{8m_h}} D_{-2m_h} \left(\frac{s}{\sqrt{2m_h}} \right), \quad (\text{B.4})$$

where $D_p(\cdot)$ is the Parabolic cylinder function. Furthermore, based on $D_p(s) \approx e^{-\frac{s^2}{4}} s^p$ [48, eq. (9.246.1)], we approximate (B.4) for $s \rightarrow \infty$ as

$$\mathcal{L}_{f_{|h_n|}}^\infty(s) = \frac{\Gamma(2m_h)(2m_h)^{m_h}}{\Gamma(m_h)} s^{-2m_h}. \quad (\text{B.5})$$

On the other hand, we denote $Q' = \sum_{k=1}^K Q'_k$ with $Q'_k = a|G_k^n| |g_k^n|$ and have

$$f_{Q'_k}(q') = \frac{1}{a} f_{Q_k} \left(\frac{q'}{a} \right). \quad (\text{B.6})$$

Then, the Laplace transform of $f_{Q'_k}(q')$ is derived as

$$\mathcal{L}_{f_{Q'_k}}(s) = \mathcal{L}_{f_{Q_k}}(as). \quad (\text{B.7})$$

Since all Q_k are i.i.d., we have

$$\mathcal{L}_{f_{Q'}}^\infty(s) = \prod_{k=1}^K \mathcal{L}_{f_{Q'_k}}^\infty(s). \quad (\text{B.8})$$

Since, $|h_n|$ and Q' are independent, we have

$$\mathcal{L}_{f_Z}^\infty(s) \approx \mathcal{L}_{f_{|h_n|}}^\infty(s) \mathcal{L}_{f_{Q'}}^\infty(s) = \frac{\Gamma(2m_h)(2m_h)^{m_h} \phi_2^K a^{-2m_s K}}{\Gamma(m_h)} s^{-2m_h - 2m_s K}. \quad (\text{B.9})$$

After carrying out the inverse Laplace transform, we have

$$f_Z^{0+}(z) \approx \phi_5 z^{2m_h + 2m_s K - 1}, \quad (\text{B.10})$$

where $\phi_5 = \frac{\Gamma(2m_h)(2m_h)^{m_h} \phi_2^K a^{-2m_s K}}{\Gamma(m_h)\Gamma(2m_h + 2m_s K)}$. Then, we have

$$F_Z^{0+}(z) \approx \xi_3 z^{2m_h + 2m_s K}, \quad (\text{B.11})$$

where $\xi_3 = \frac{\phi_5}{2m_h + 2m_s K}$.

Ordered channel gain: Based on order statistics [49], the CDF of Z_n for $z \rightarrow 0^+$ can be approximated as

$$F_{Z_n}^{0+}(z) \approx \frac{N!}{(N-n)!(n-1)!} \sum_{i=0}^{N-n} \binom{N-n}{i} \frac{(-1)^i}{n+i} \left(F_Z^{0+}(z)\right)^{n+i}. \quad (\text{B.12})$$

This completes the proof.

ACKNOWLEDGMENT

The authors would like to thank Professor Mohamed-Slim Alouini from King Abdullah University of Science and Technology (KAUST) for helping us improve the system model design.

REFERENCES

- [1] Z. Ding, X. Lei, G. K. Karagiannidis, R. Schober, J. Yuan, and V. K. Bhargava, "A survey on non-orthogonal multiple access for 5G networks: Research challenges and future trends," *IEEE J. Sel. Areas Commun.*, vol. 35, no. 10, pp. 2181–2195, Jul. 2017.
- [2] J. Montalban, P. Scopelliti, M. Fadda, E. Iradier, C. Desogus, P. Angueira, M. Murrioni, and G. Araniti, "Multimedia multicast services in 5G networks: Subgrouping and non-orthogonal multiple access techniques," *IEEE Commun. Mag.*, vol. 56, no. 3, pp. 91–95, Mar. 2018.
- [3] Y. Liu, Z. Qin, M. Elkashlan, Y. Gao, and L. Hanzo, "Enhancing the physical layer security of non-orthogonal multiple access in large-scale networks," *IEEE Trans. Wireless Commun.*, vol. 16, no. 3, pp. 1656–1672, Mar. 2017.
- [4] Y. Liu, Z. Qin, M. Elkashlan, Z. Ding, A. Nallanathan, and L. Hanzo, "Non-orthogonal multiple access for 5G and beyond," *Proc. IEEE*, vol. 105, no. 12, pp. 2347–2381, Dec. 2017.
- [5] Y. Liu, X. Liu, X. Mu, T. Hou, J. Xu, Z. Qin, M. Di Renzo, and N. Al-Dhahir, "Reconfigurable intelligent surfaces: Principles and opportunities." [Online]. Available: <https://arxiv.org/abs/2007.03435>
- [6] B. Ning, Z. Chen, W. Chen, Y. Du, and J. Fang, "Channel estimation and hybrid beamforming for reconfigurable intelligent surfaces assisted THz communications." [Online]. Available: <https://arxiv.org/abs/1912.11662>

- [7] H. Shen, W. Xu, S. Gong, Z. He, and C. Zhao, "Secrecy rate maximization for intelligent reflecting surface assisted multi-antenna communications," *IEEE Commun. Lett.*, vol. 23, no. 9, pp. 1488–1492, Sep. 2019.
- [8] G. Zhou, C. Pan, H. Ren, K. Wang, and A. Nallanathan, "A framework of robust transmission design for IRS-aided MISO communications with imperfect cascaded channels." [Online]. Available: <https://arxiv.org/abs/2001.07054>
- [9] L. Dong and H.-M. Wang, "Secure MIMO transmission via intelligent reflecting surface," *IEEE Wireless Commun. Lett.*, vol. 9, no. 6, pp. 787–790, Jun. 2020.
- [10] K. Feng, Q. Wang, X. Li, and C.-K. Wen, "Deep reinforcement learning based intelligent reflecting surface optimization for MISO communication systems," *IEEE Wireless Commun. Lett.*, vol. 9, no. 5, pp. 745–749, May 2020.
- [11] Q. Wu and R. Zhang, "Towards smart and reconfigurable environment: Intelligent reflecting surface aided wireless network," *IEEE Commun. Mag.*, vol. 58, no. 1, pp. 106–112, Jan. 2020.
- [12] Z. Wang, L. Liu, and S. Cui, "Channel estimation for intelligent reflecting surface assisted multiuser communications: Framework, algorithms, and analysis," *IEEE Trans. Wireless Commun.*, vol. 19, no. 10, pp. 6607–6620, Oct. 2020.
- [13] M. Cui, G. Zhang, and R. Zhang, "Secure wireless communication via intelligent reflecting surface," *IEEE Wireless Commun. Lett.*, vol. 8, no. 5, pp. 1410–1414, Oct. 2019.
- [14] N. Otao, Y. Kishiyama, and K. Higuchi, "Performance of non-orthogonal access with SIC in cellular downlink using proportional fair-based resource allocation," in *Proc. Int. Symp. Wireless Commun. Syst. (ISWCS)*, Paris, France, Aug. 2012, pp. 1–6.
- [15] Y. Saito, Y. Kishiyama, A. Benjebbour, T. Nakamura, A. Li, and K. Higuchi, "Non-orthogonal multiple access (NOMA) for cellular future radio access," in *Proc. IEEE Veh. Technol. Conf. (VTC)*, Dresden, Germany, Jun. 2013, pp. 1–5.
- [16] Y. Saito, A. Benjebbour, Y. Kishiyama, and T. Nakamura, "System-level performance evaluation of downlink non-orthogonal multiple access (NOMA)," in *Proc. IEEE Int. Symp. Pers., Indoor, and Mobile Radio Commun. (PIMRC)*, London, UK, Sep. 2013, pp. 611–615.
- [17] Z. Ding, Z. Yang, P. Fan, and H. V. Poor, "On the performance of non-orthogonal multiple access in 5G systems with randomly deployed users," *IEEE Signal Process. Lett.*, vol. 21, no. 12, pp. 1501–1505, Dec. 2014.
- [18] Z. Ding, P. Fan, and H. V. Poor, "Impact of user pairing on 5G nonorthogonal multiple-access downlink transmissions," *IEEE Trans. Veh. Technol.*, vol. 65, no. 8, pp. 6010–6023, Aug. 2016.
- [19] J. A. Oviedo and H. R. Sadjadpour, "A fair power allocation approach to NOMA in multi-user SISO systems," *IEEE Trans. Veh. Technol.*, vol. 66, no. 9, pp. 7974–7985, Sep. 2017.
- [20] P. Xu, Z. Ding, X. Dai, and H. V. Poor, "A new evaluation criterion for non-orthogonal multiple access in 5G software defined networks," *IEEE Access*, vol. 3, pp. 1633–1639, Sep. 2015.
- [21] Y. Liu, Z. Ding, M. ElKashlan, and H. V. Poor, "Cooperative non-orthogonal multiple access with simultaneous wireless information and power transfer," *IEEE J. Sel. Areas Commun.*, vol. 34, no. 4, pp. 938–953, Apr. 2016.
- [22] W. Shi, X. Zhou, L. Jia, Y. Wu, F. Shu, and J. Wang, "Enhanced secure wireless information and power transfer via intelligent reflecting surface." [Online]. Available: <https://arxiv.org/abs/1911.01001>
- [23] Ö. Özdoğan, E. Björnson, and E. G. Larsson, "Intelligent reflecting surfaces: Physics, propagation, and pathloss modeling," *IEEE Wireless Commun. Lett.*, vol. 9, no. 5, pp. 581–585, May 2020.
- [24] E. Björnson, Ö. Özdoğan, and E. G. Larsson, "Intelligent reflecting surface versus decode-and-forward: How large surfaces are needed to beat relaying?" *IEEE Wireless Commun. Lett.*, vol. 9, no. 2, pp. 244–248, Feb. 2020.
- [25] J. Lyu and R. Zhang, "Spatial throughput characterization for intelligent reflecting surface aided multiuser system," *IEEE Wireless Commun. Lett.*, vol. 9, no. 6, pp. 834–838, Jun. 2020.
- [26] H. Wang, Z. Zhang, B. Zhu, J. Dang, L. Wu, L. Wang, K. Zhang, and Y. Zhang, "Performance of

- wireless optical communication with reconfigurable intelligent surfaces and random obstacles.” [Online]. Available: <https://arxiv.org/abs/2001.05715>
- [27] Z. Zhang, Y. Cui, F. Yang, and L. Ding, “Analysis and optimization of outage probability in multi-intelligent reflecting surface-assisted systems.” [Online]. Available: <https://arxiv.org/abs/1909.02193>
- [28] X. Yu, D. Xu, and R. Schober, “MISO wireless communication systems via intelligent reflecting surfaces,” in *Proc. IEEE/CIC Int. Conf. Commun. China (ICCC)*, Changchun, China, Aug. 2019, pp. 735–740.
- [29] Q. Wu and R. Zhang, “Intelligent reflecting surface enhanced wireless network via joint active and passive beamforming,” *IEEE Trans. Wireless Commun.*, vol. 18, no. 11, pp. 5394–5409, Nov. 2019.
- [30] H. Han, J. Zhao, D. Niyato, M. Di Renzo, and Q.-V. Pham, “Intelligent reflecting surface aided network: Power control for physical-layer broadcasting,” in *Proc. IEEE Int. Conf. Commun. (ICC)*, Dublin, Ireland, Jun. 2020, pp. 1–7.
- [31] X. Guan, Q. Wu, and R. Zhang, “Intelligent reflecting surface assisted secrecy communication: Is artificial noise helpful or not?” *IEEE Wireless Commun. Lett.*, vol. 9, no. 6, pp. 778–782, Jun. 2020.
- [32] J. Xu, W. Xu, and A. L. Swindlehurst, “Discrete phase shift design for practical large intelligent surface communication,” in *Proc. IEEE Pacific Rim Conf. Commun., Comput. and Signal Process. (PACRIM)*, Victoria, BC, Canada, Aug. 2019, pp. 1–5.
- [33] H. Guo, Y.-C. Liang, J. Chen, and E. G. Larsson, “Weighted sum-rate maximization for intelligent reflecting surface enhanced wireless networks,” in *Proc. IEEE Global Commun. Conf. (GLOBECOM)*, Waikoloa, HI, USA, Dec. 2019, pp. 1–6.
- [34] C. You, B. Zheng, and R. Zhang, “Channel estimation and passive beamforming for intelligent reflecting surface: Discrete phase shift and progressive refinement,” *IEEE J. Sel. Areas Commun.*, vol. 38, no. 11, pp. 2604–2620, Nov. 2020.
- [35] S. Abeywickrama, R. Zhang, Q. Wu, and C. Yuen, “Intelligent reflecting surface: Practical phase shift model and beamforming optimization,” *IEEE Trans. Commun.*, vol. 68, no. 9, pp. 5849–5863, Sep. 2020.
- [36] Q. Wu and R. Zhang, “Beamforming optimization for intelligent reflecting surface with discrete phase shifts,” in *Proc. IEEE Int. Conf. Acoust., Speech and Signal Process. (ICASSP)*, Brighton, UK, May 2019, pp. 7830–7833.
- [37] —, “Beamforming optimization for wireless network aided by intelligent reflecting surface with discrete phase shifts,” *IEEE Trans. Commun.*, vol. 68, no. 3, pp. 1838–1851, Mar. 2019.
- [38] J. Ye, S. Guo, and M.-S. Alouini, “Joint reflecting and precoding designs for SER minimization in reconfigurable intelligent surfaces assisted MIMO systems,” *IEEE Trans. Wireless Commun.*, vol. 19, no. 8, pp. 5561–5574, Aug. 2020.
- [39] Z. Ding and H. V. Poor, “A simple design of IRS-NOMA transmission,” *IEEE Commun. Lett.*, vol. 24, no. 5, pp. 1119–1123, May 2020.
- [40] Z. Ding, R. Schober, and H. V. Poor, “On the impact of phase shifting designs on IRS-NOMA,” *IEEE Wireless Commun. Lett.*, vol. 9, no. 10, pp. 1596–1600, Oct. 2020.
- [41] J. Zhu, Y. Huang, J. Wang, K. Navaie, and Z. Ding, “Power efficient IRS-assisted NOMA.” [Online]. Available: <https://arxiv.org/abs/1912.11768>
- [42] M. Fu, Y. Zhou, and Y. Shi, “Intelligent reflecting surface for downlink non-orthogonal multiple access networks,” in *Proc. IEEE Global Commun. Conf. (GLOBECOM)*, Waikoloa, HI, USA, Dec. 2019, pp. 1–6.
- [43] G. Yang, X. Xu, and Y.-C. Liang, “Intelligent reflecting surface assisted non-orthogonal multiple access,” in *Proc. IEEE Wireless Commun. and Netw. Conf. (WCNC)*, Seoul, South Korea, May 2020, pp. 1–6.
- [44] X. Liu, Y. Liu, Y. Chen, and H. V. Poor, “RIS enhanced massive non-orthogonal multiple access networks: Deployment and passive beamforming design.” [Online]. Available: <https://arxiv.org/abs/2001.10363>
- [45] T. Hou, Y. Liu, Z. Song, X. Sun, Y. Chen, and L. Hanzo, “Reconfigurable intelligent surface aided NOMA networks,” *IEEE J. Sel. Areas Commun.*, vol. 38, no. 11, pp. 2575–2588, Nov. 2020.

- [46] Y. Cheng, K. H. Li, Y. Liu, K. C. Teh, and H. V. Poor, "Downlink and uplink intelligent reflecting surface aided networks: NOMA and OMA." [Online]. Available: <https://arXiv:2005.00996>
- [47] N. Bhargav, C. R. N. da Silva, Y. J. Chun, É. J. Leonardo, S. L. Cotton, and M. D. Yacoub, "On the product of two κ - μ random variables and its application to double and composite fading channels," *IEEE Trans. Wireless Commun.*, vol. 17, no. 4, pp. 2457–2470, Apr. 2018.
- [48] I. S. Gradshteyn and I. M. Ryzhik, *Table of Integrals, Series, and Products*, 7th ed. Amsterdam, The Netherlands: Elsevier, 2007.
- [49] H. A. David and H. N. Nagaraja, *Order Statistics*, 3rd ed. Hoboken, NJ, USA: Wiley, 2004.